Air-bridge Si Thermophotovoltaic Cell with High Photon Utilization

Byungjun Lee[1†], Rebecca Lentz[1†], Tobias Burger[2], Bosun Roy-Layinde[2], Jihun Lim[1], R. Matthew Zhu[1], Dejiu Fan[1], Andrej Lenert[2] and Stephen R. Forrest[1,3]*

[1]Department of Electrical Engineering, University of Michigan, 1301 Beal Ave, Ann Arbor, MI 48109

[2]Department of Chemical Engineering, University of Michigan, 2300 Hayward St, Ann Arbor, MI 48109

[3]Department of Physics, University of Michigan, 450 Church St, Ann Arbor, MI 48109

[†]These authors contributed equally to this work

Corresponding Author

Stephen Forrest

Department of Electrical Engineering and Computer Science, University of Michigan, Ann Arbor, Michigan 48109, United States

Email: stevefor@umich.edu

ABSTRACT

Thermophotovoltaic (TPV) cells convert photons emitted from hot surfaces into electrical power. Unlike solar cells, TPV cells can be placed in close proximity to the heat source, allowing below-bandgap (i.e., out-of-band, OOB) photons to be reflected and re-absorbed by the emitter. As the reflectance of OOB photons approaches unity, the spectral efficiency of the TPV becomes increasingly insensitive to the bandgap of the cell and the source temperature. Here, we employ air-bridge structures with a lateral junction Si TPV cell as a means of increasing OOB reflectivity, which allows for efficient operation at low thermal source temperatures that were long inaccessible to efficient Si TPV power generation. The devices exhibit an OOB reflectance of 98.0 ± 0.1% and an air-bridge scalability to at least 6 cm x 6 cm. Compared to devices with a Au back surface reflector (BSR), devices featuring an air-bridge BSR exhibit a 25% relative increase in power conversion efficiency at a thermal source temperature of 1988K. Such performance improvements in TPV cells made with scalable and relatively low-cost Si can potentially expedite the widespread use of TPV systems in both energy storage and generation systems.

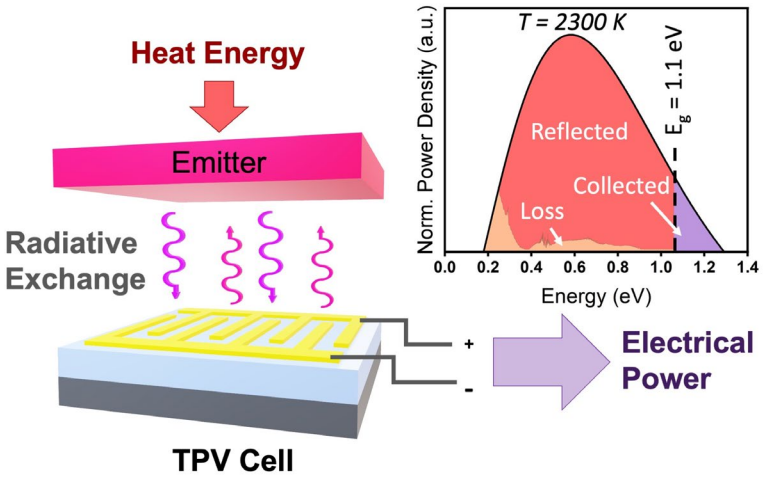

MAIN TEXT

Conversion of heat to electricity plays an important role in various energy applications including waste heat scavenging[1], distributed generation[2-4], thermal energy storage[5,6] and direct solar energy conversion.[7-11] TPV cells are used in such applications to convert radiated photons from high temperature sources into electrical power via the photovoltaic effect. As the emitter and cell can be placed in close proximity, reflecting and recycling photons with insufficient energy to excite electronic transitions can produce a significant improvement in power conversion efficiency.[12-13] Such wavelength-selective photon recovery can be achieved using a front surface filter (FSF), or a back surface reflector (BSR).[12] Calculations show that with an out-of-band (OOB) reflectance of >99%, the spectral efficiency of the TPV system becomes increasingly insensitive to the emitter temperature or cell bandgap.[14]

While the OOB reflectance of metal BSRs[15-17], photonic crystals (PhC)[18] and Bragg/plasma filters[19] remain below 95%, Fan, et al. recently demonstrated an $In_{0.53}Ga_{0.47}As$ (InGaAs) air-bridge TPV cell with ~99% OOB reflectance, which resulted in an 8% increase in power conversion efficiency compared to the same device with a Au BSR.[14] With this high OOB reflectance, it was suggested that efficient TPV cells based on low-cost, but higher bandgap semiconductors such as Si can potentially be paired with relatively low temperature emitters (1000-1500K).

There are few previous works on Si TPV cells[20-24] due to its relatively high bandgap compared to InGaAs and GaSb. Reports on Si TPV include that of Yeng, et al.[25] who demonstrated a power conversion efficiency of 6.4% for a conventional Si PV cell with a PhC selective filter paired with a 1660K 2D tantalum PhC emitter. Swanson[15] reported a Si TPV cell with an SiO_2/Ag BSR that exhibited ~95% OOB reflectance and a power conversion efficiency of 29% using a 2300 K

broadband emitter. Dielectric spacers such as these can theoretically achieve a high R_{out}, but are limited by absorption in the far infrared (see Supplemental Information).

Here, we demonstrate a Si TPV cell with an air-bridge BSR achieving an OOB reflectance of 98.0 ± 0.1%. To minimize free carrier absorption (FCA), we use a lateral *p-n* junction along with reflective Au contacts on the surface of a 300 µm thick p-type Si substrate with low doping (p ~ 10^{15} cm^{-3}). The wafer thickness is chosen for ease of handling during fabrication. Figures 1(a) and (b) show schematic illustrations of the device cross-section and top view, respectively. The interdigitated top contacts have a width, w = 20 µm, and spacing, d = 60 µm, where d is smaller than the electron diffusion length (100-250 µm) in p-type Si.[26-28]

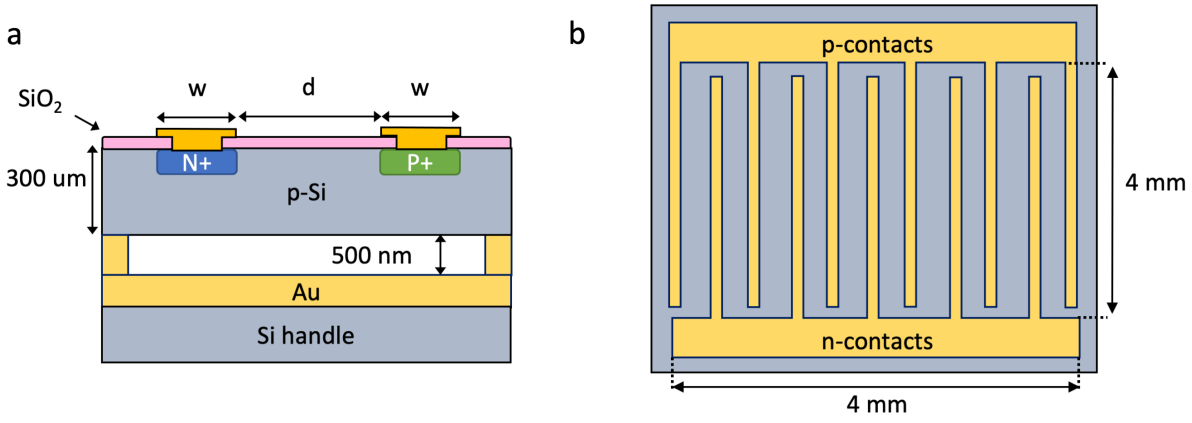

Figure 1. (a) Cross-section schematic of the Si TPV cell structure. Here, w indicates the contact finger width and d the spacing between contact fingers. (b) Top view of the contact design and active area dimensions.

We fabricated a 6 cm x 6 cm Si air-bridge, supported by 7 µm wide Au grids spaced 100 µm apart to verify the scalability of the fabrication process. Figure 2(a) shows the sample after cold-weld bonding[29] to a 4" Si handle wafer coated with Au. Figure 2(b) shows a scanning electron

microscope image of the cleaved air-bridge cross section and its uniformity over the sample. The inset is a detailed image of the air-bridge support grids and air gap height.

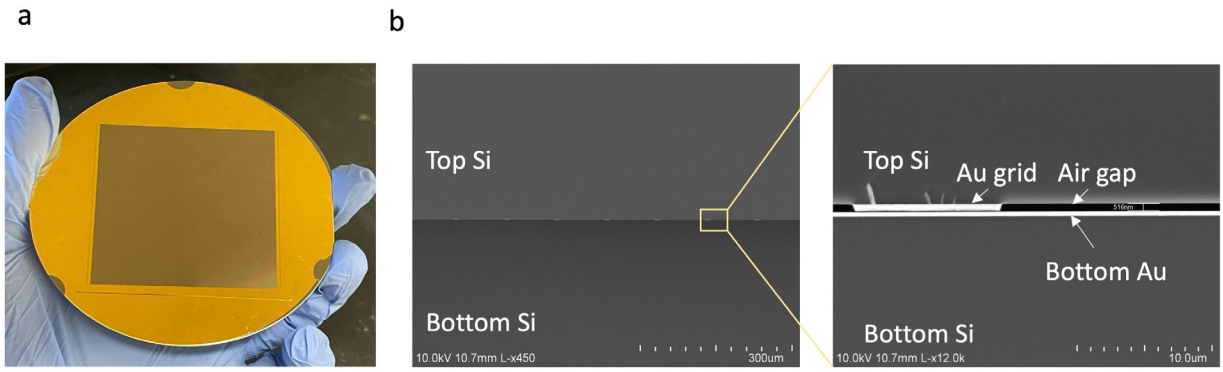

Figure 2. (a) Micrograph of a 6 cm × 6 cm air-bridge structure bonded onto a 4" Si handle wafer. (b) Scanning electron microscope image of a cleaved cross section of the air-bridge. *Inset*: Enlarged view of the air gap and Au grid support.

To minimize surface recombination loss common to lateral *p-n* junction structures, passivation of the top surface is critical. For this purpose, we deposited a 165 nm thick SiO_2 layer via chemical vapor deposition (CVD) at 425°C. This passivation layer also acts as a single layer anti-reflective coating (ARC), which is optimized for long wavelength photons by calculating the thin-film transmission via the transfer matrix method[30] and weighting it to a 2300K blackbody spectrum.

As noted above, high OOB reflectance is critical for achieving high power conversion efficiency. Reflectance is increased by introducing an air gap between the back of the cell and the Au reflector.[14] This maximizes the index mismatch at the reflecting interface compared to the Si-metal interface of a metal BSR. Simulation results using the transfer matrix method[30] indicate a maximum OOB reflectance of 98.9% for a 500nm thick air-bridge BSR at an emitter temperature of 2300K, compared to the 96.1% achievable with a Au BSR.[31]

Figure 3 shows the external quantum efficiency (*EQE*) for an air-bridge Si cell, the simulated emission spectrum of a 2300K blackbody, and the device absorptance vs. wavelength measured using Fourier-transform infrared (FTIR) spectroscopy. The spectrum shows a significant decrease in the cell absorptance corresponding to an increase in OOB reflectance for the air-bridge. When weighted by a 1988K blackbody emission spectrum, the air-bridge cell exhibits an average reflectance of 98.0 ± 0.1% compared to 95.3 ± 0.5% for to the Au BSR cell – a difference that is consistent with optical simulations. The air-bridge cell has a maximum *EQE* = 83.5 ± 0.3% at a wavelength of 0.75 µm.

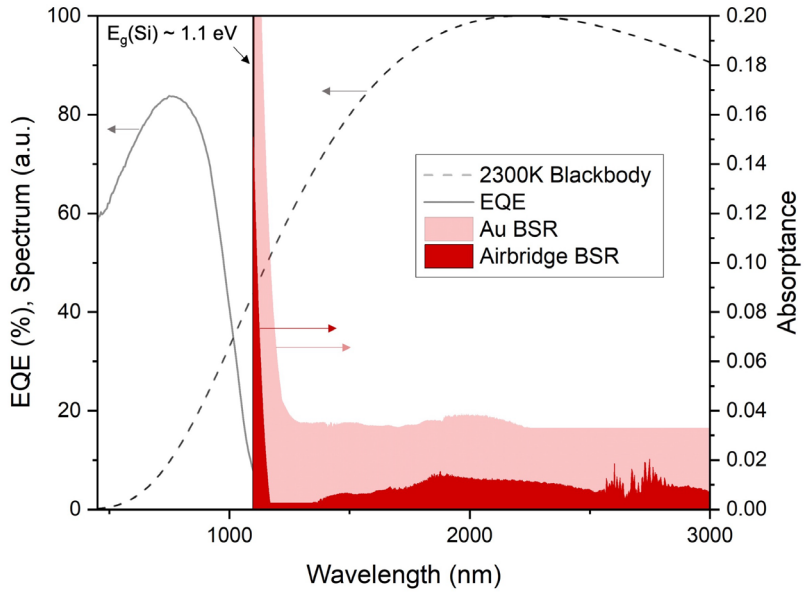

Figure 3. Absorptance measured via FTIR for the air-bridge and Au back surface reflector (BSR) devices, the external quantum efficiency (*EQE*) of a 4 mm x 4 mm device with 20 µm x 60 µm contact grids, and the simulated normalized spectrum of a 2300K blackbody emitter.

Current density-voltage (*J-V*) characteristics of the air-bridge and Au BSR devices were measured at several temperatures (T_h) of a SiC emitter (globar) at a constant view factor ($F_{V,\,Au\,BSR}$

= 0.37 ± 0.03 and $F_{V,\text{air-bridge}}$ = 0.29 ± 0.03). Figure 4(a) shows the *J-V* characteristics and generated power density vs. voltage for a 4 cm x 4 cm active area air-bridge Si TPV cell with w = 20 μm and d = 60 μm top contact grids at T_h = 1988K, while Figure 4(b) shows the open circuit voltage (V_{OC}) vs. the short-circuit current density (J_{SC}) at several temperatures. As T_h increases from 1639K to 1988K, V_{OC} increases from 590 mV to 630 mV, and J_{SC} from 125 mA/cm^2 to 923 mA/cm^2.

The power conversion efficiency is calculated using $\eta = \frac{P_{MPP}}{P_{abs}}$, where P_{MPP} is the measured power at the maximum power point, and P_{abs} is the power absorbed by the Si cell, which is equal to the power incident minus the power reflected.[14] This efficiency metric (referred to as "pairwise efficiency" elsewhere[32]) describes the power conversion efficiency of the device and emitter pair without factoring in losses associated with a non-ideal TPV enclosure. In Figure 4(c), we compare the efficiency of the air-bridge cell and the Au BSR cell with increasing temperature T_h. For both devices, we observe a nearly linear increase with T_h, with the air-bridge cell outperforming the Au BSR cell at all temperatures. At 1988K, the air-bridge cell has an efficiency of 18.9 ± 0.4%, which is a 25% relative increase from the Au BSR cell efficiency of 15.1 ± 0.3%. This improvement is attributed to the increased OOB reflectance of the air-bridge architecture.

To compare the Si air-bridge cell to previous work, we calculate the spectral efficiency, *SE* (see Methods), which describes how well the cells utilize the emitter spectrum.[14] Figure 4(d) shows the calculated spectral efficiencies of the Si air-bridge and Au BSR cells vs. temperature and band gap. At 1988K, the air-bridge cell shows a spectral efficiency of 63.2 ± 0.1%, compared to 49.7 ± 0.4% for the Au BSR cell. Notably, the air-bridge cell measured at T_h = 1988K outperforms the 56% spectral efficiency achieved by Swanson at T_h = 2300K (star) and indicates a trend for even higher spectral efficiency (~70%) at the same temperature.[15] The spectral efficiency is related to

the power conversion efficiency via $\eta = SE \times IQE \times vf \times FF$, where the internal quantum efficiency (*IQE*) is the ratio of *EQE* to in-band absorption (A_{in}), the voltage factor, *vf,* is the ratio of open circuit voltage V_{OC} to the bandgap voltage V_g. The values of fill factor (*FF*) and V_{OC} are extracted from the *J-V* characteristics. When $IQE \times vf \times FF$ is held constant, the 13.5% (absolute) increase in spectral efficiency from the Au BSR to the air-bridge accounts for a 4% (absolute) increase in η, a value that is consistent with the measured results. Even with its higher spectral efficiency, the air-bridge cell operates at only ~30% of the radiative limit at 1988K.[32] Improved material quality, device passivation, and contact design, Si TPV cells could potentially approach 70% of the radiative limit, as achieved by commercial solar cells.[33] With this electrical performance, the difference in spectral efficiency becomes more critical, accounting for a 9.5% increase in PCE from the Au BSR to the air-bridge. For an air-bridge cell with a 98% OOB reflectance and comparable carrier management to Si solar cells, a conversion efficiency of 45% at 2000K is achievable.[32]

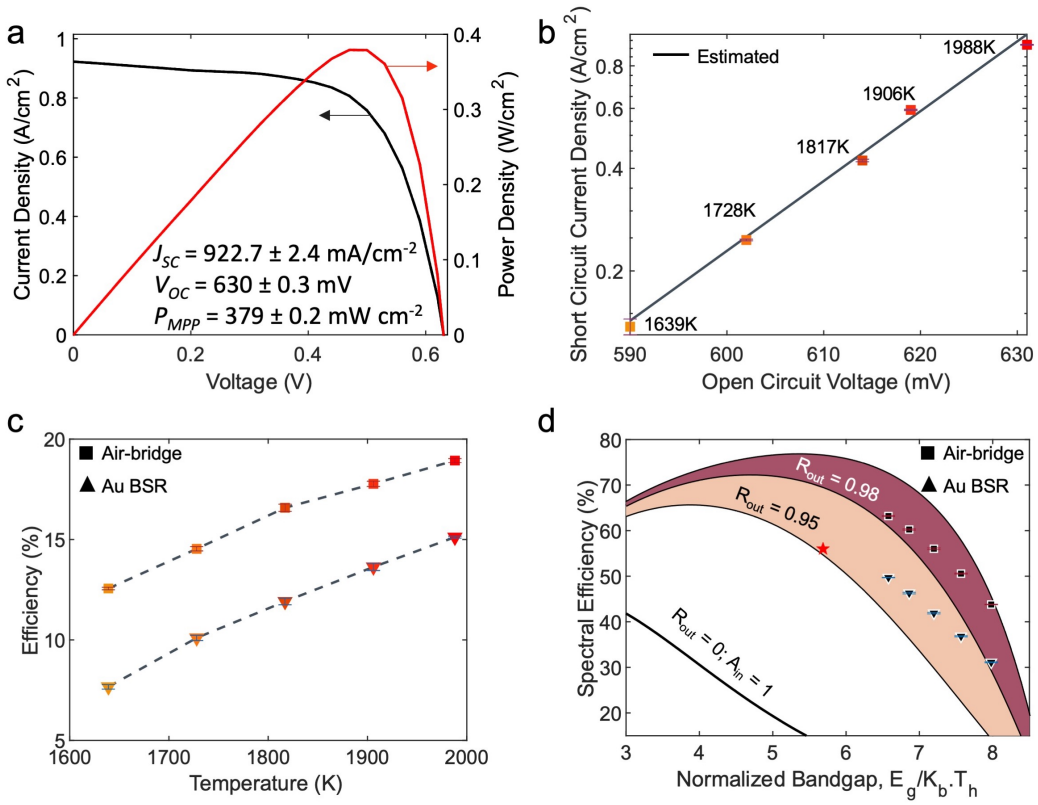

Figure 4. (a) Current density and power density vs. voltage for the air-bridge Si TPV at 1988K. (b) Short circuit current density (J_{SC}) vs. open circuit voltage (V_{OC}) for several emitter temperatures. (c) TPV power conversion efficiency vs. temperature for air-bridge (squares) and Au BSR (triangles) devices. (d) Spectral efficiency and conversion efficiency for air-bridge and Au BSR devices vs. energy gap normalized to the thermal energy, E_g/k_BT, where k_B is Boltzmann's constant and T is temperature. Shaded regions depict limits for possible spectral efficiencies with Rout = 0, 0.95 and 0.98.

In conclusion, we demonstrated a Si TPV cell with an air-bridge back surface reflector, increasing the average OOB reflectance from the 95.3 ± 0.5% of a conventional Au BSR to 98.0 ± 0.1%. This OOB reflectance increase is responsible for a relative 25% increase in power conversion efficiency at 1988K. By implementing the air-bridge BSR with low-cost, high-

scalability Si, this work provides a critical advance toward the widespread adoption of TPVs for a range of applications. Combined with the optimized cell design techniques of industrial and research-grade solar cells, the Si air-bridge TPV cell shows a near-term path for conversion efficiencies as high as 45%.

EXPERIMENTAL METHODS

Device Fabrication

Before all oxidation or diffusion steps, the double-side polished p-type ($p \sim 10^{15}$ cm^{-3}) Si wafers are subjected to a standard RCA cleaning process[34] starting with a 10 min clean in NH_4OH and H_2O_2, followed by an HF dip and a final 10 min clean in HCl and H_2O_2. Next, a thermal oxide mask is grown via wet oxidation at 1000°C, and patterned using standard photolithography and deep reactive ion etching (DRIE). Boron is diffused at 1050°C for 2 h using Techneglas GS139 boron sources. The oxide is stripped in HF and replaced by a second low pressure chemical vapor deposited (LPCVD) oxide at 900°C, which is then patterned using standard photolithography and DRIE. Phosphorous is diffused from a $POCl_3$ source at 950°C for 30 min, followed by a 5 min drive-in. After oxide removal in HF, a final low temperature LPCVD oxide is deposited at 425°C to avoid further dopant migration. This oxide provides surface passivation and acts as an anti-reflective coating (ARC). The oxide is patterned and wet etched in HF followed by e-beam deposition of a Ti/Pt/Al/Pt/Au (5/30/1500/30/200 nm) contact layer that is patterned by metal lift-off. Finally, a Ti/Au (5/500 nm) support grid is deposited on the back surface of the device and bonded onto a Au/Si handle via cold welding[29] under 2MPa at 150°C for 3 min to form the air-

bridge. The Au BSR control samples are formed by sputtering Au on the backside of the cell and cold-weld bonding to the Au/Si handle.[29]

External Quantum Efficiency Measurement

The cells were placed under monochromatic illumination, chopped at 200Hz, and coupled into a multimode SMA to a bare fiber optic cable patch. The light illumination power is calibrated using a reference 818-UV/DB Si detector (Newport) from 400 to 1100nm, and the output signal from the TPV cell is measured by an SR830 lock-in amplifier. The current was normalized to the open area ratio to compensate for contact grid shadowing.

Spectral Reflectance

Fourier-transform infrared (FTIR) spectroscopy is used to measure the reflectance of the Si air-bridge BSR and Au BSR cells. The range of incident angles is 18° – 41°. The techniques used for spectral averaging are described in [14].

Illuminated *J-V* Characteristics

The *J-V* characteristics are measured using a Keithley 2401 source meter. Emitter temperature is regulated by varying the electrical input power to a SiC Globar emitter, while the cell temperature is maintained at 25ºC using a chilled water loop containing water and ethylene glycol mixture. The temperature of the emitter is determined through FTIR characterization and fitting of the emission spectrum using previous procedures.[14]

Spectral Efficiency Calculation

Spectral efficiency is calculated using:

$$SE = \frac{E_g \int_{E_g}^{\infty} \varepsilon_{eff}(E) b(E, T_h) dE}{\int_0^{\infty} \varepsilon_{eff}(E) E b(E, T_h) dE}$$

where b(E, T_h) is the spectral photon flux of the emitter, E_g is the absorber band gap, and ε_{eff} is the effective emissivity of the cavity formed by the emitter and the TPV cell. Effective emissivity is calculated by previous procedures[14] using the FTIR measurements over 18°–41° and emitter emissivity measurements over 0°–30°.

AUTHOR INFORMATION

http://websites.umich.edu/~ocm/

https://lenert.engin.umich.edu/

Notes

The authors declare no competing financial interest.

SUPPORTING INFORMATION

Illuminated I-V curves and parameters, series and shunt resistances, out-of-band reflectance simulation data and angular dependence, external quantum efficiencies, simulation and experimental comparison of air-bridge to alternate dielectric reflectors and back passivated structures

ACKNOWLEDGMENT

This material is based upon work supported by the National Science Foundation under Grant Number 2018572.

REFERENCES

(1) Licht, A.; Pfiester, N.; Demeo, D.; Chivers, J.; Vandervelde, T. E. A Review of Advances in Thermophotovoltaics for Power Generation and Waste Heat Harvesting. *MRS Adv*. **2019**, *4*, 41–42, 2271–2282.

(2) Fraas, L. M.; Avery, J. E.; Huang, H. X. Thermophotovoltaic Furnace-Generator for the Home Using Low Bandgap GaSb Cells. *Semicond. Sci. Technol*. **2003**, *18*, 5, 247–253.

(3) Bianchi, M.; Ferrari, C.; Melino, F.; Peretto, A. Feasibility Study of a Thermo-Photo-Voltaic System for CHP Application in Residential Buildings," *Appl. Energy* **2012**, *97*, 704–713.

(4) Durisch, W.; Bitnar, B. Novel Thin Film Thermophotovoltaic System," *Sol. Energy Mater. Sol. Cells* **2010**, *94*, 6, 960–965.

(5) Datas, A.; Ramos, A.; Martí, A.; del Cañizo, C.; Luque, A. Ultra High Temperature Latent Heat Energy Storage and Thermophotovoltaic Energy Conversion. *Energy* **2016**, *107*, 542–549.

(6) Amy, C.; Seyf, H. R.; Steiner, M. A.; Friedman, D. J.; Henry, A.; Thermal Energy Grid Storage Using Multi-Junction Photovoltaics. *Energy Environ. Sci.* **2019**, *12*, 1.

(7) Harder N. P.; Würfel, P. Theoretical Limits of Thermophotovoltaic Solar Energy Conversion. *Semicond. Sci. Technol*. **2003**, *18*, 5, S151.

(8) Rephaeli, E.; Fan, S. Absorber and Emitter for Solar Thermo-photovoltaic Systems to Achieve Efficiency Exceeding the Shockley-Queisser Limit. *Opt. Express* **2009**, *17*, 15145.

(9) Lenert, A.; Bierman, D. M.; Nam, Y.; Chan, W. R.; Celanović, I.; Soljačić, M.; Wang, E. N. A Nanophotonic Solar Thermophotovoltaic Device," *Nat. Nanotechnol*. **2014**, *9*, 2, 126–130.

(10) Ungaro, C.; Gray, S. K.; Gupta, M. C. Solar Thermophotovoltaic System Using Nanostructures. *Opt. Express* **2015**, *23*, 19, A1149.

(11) Bierman, D. M.; et al. Enhanced Photovoltaic Energy Conversion Using Thermally Based Spectral Shaping. *Nat. Energy* **2016**, *1*, 6, 1–7.

(12) Burger, T.; Sempere, C.; Lenert, A. Thermophotovoltaic Energy Conversion: Materials and Device Engineering. *Nanoscale Energy Transport* **2020**, 17–26.

(13) Burger, T.; Fan, D.; Lee, K.; Forrest, S. R.; Lenert, A. Thin-Film Architectures with High Spectral Selectivity for Thermophotovoltaic Cells. *ACS Photonics* **2018**, *5*, 7, 2748–2754.

(14) Fan, D.; Burger, T.; McSherry, S.; Lee, B.; Lenert, A.; Forrest, S. R. Near-Perfect Photon Utilization in an Air-bridge Thermophotovoltaic Cell. *Nature* **2020**, *586*, 7828, 237–241.

(15) Swanson, R. M. Recent Developments in Thermophotovoltaic Conversion. *International Electron Devices Meeting* **1980**, 186–189.

(16) Omair, Z.; Scranton, G.; Pazos-Outón, L. M.; Xiao, T. P.; Steiner, M. A.; Ganapati, V.; Peterson, P. F.; Holzrichter, J.; Atwater, H.; Yablonovitch, E. Ultraefficient Thermophotovoltaic Power Conversion by Band-Edge Spectral Filtering. *Proc. Natl. Acad. Sci. U. S. A*. **2019**, *116*, 31, 15356–15361.

(17) Wernsman, B.; Sierglej, R. R.; Link, S. D.; Mahorter, R. G. Greater Than 20% Radiant Heat Conversion Efficiency of a Thermophotovoltaic Radiator/Module System Using Reflective Spectral Control. *IEEE Trans. Electron Devices* **2004**, *51*, 3, 512–515.

(18) Shemelya, C; Demeo, D. F.; Vandervelde, T. E. Two Dimensional Metallic Photonic Crystals for Light Trapping and Anti-reflective Coatings in Thermophotovoltaic Applications. *Appl. Phys. Lett*. **2014**, *104*, 2, 1–4.

(19) Fourspring, P. M.; DePoy, D. M.; Rahmlow, T. D.; Lazo-Wasem, J. E.; Gratrix, E. J. Optical Coatings for Thermophotovoltaic Spectral Control. *Appl. Opt*. **2006**, *45*, 7, 1356–1358.

(20) Bitnar, B.; Mayor, J. C.; Durisch, W.; Meyer, A.; Palfinger, G.; von Roth, F.; Sigg, H. Record Electricity-to-Gas Power Efficiency of a Silicon Solar Cell Based TPV System. *AIP Conf. Proc*. **2003**, *653*, 1, 18.

(21) Gordon, R.; Stone, K.; Garboushian, V. Design Considerations for the Development of a Highly Reliable Densely Packed Photovoltaic Array for TPV Applications. *Conf. Rec. IEEE Photovolt. Spec. Conf.* **2002**, 947–950.

(22) Nelson, R. E. TPV Systems and State-of-Art Development. *AIP Conf. Proc*. **2003**, *653*, 1, 3.

(23) Bitnar, B.; Durisch, W.; Meyer, A; Palfinger, G. New Flexible Photocell Module for Thermophotovoltaic Applications. *AIP Conf. Proc*. **2003**, *653*, 1, 465.

(24) Palfinger, G.; Bitnar, B.; Durisch, W.; Mayor, J.; Grützmacher, D.; Gobrecht, J. Cost Estimates of Electricity from a TPV Residential Heating System. *AIP Conf. Proc*. **2003**, *653*, 1, 29.

(25) Yeng Y. X.; Chan, W. R.; Rinnerbauer, V.; Stelmakh, V. Photonic Crystal Enhanced Silicon Cell Based Thermophotovoltaic Systems. *Opt. Express* **2015**, *23*, 3, A157.

(26) Reiss, J. H.; King, R. R.; and Mitchell, K. W.; Characterization of Diffusion Length Degradation in Czochralski Silicon Solar Cells. *Appl. Phys. Lett*. **1996**, *68*, 3302-3304.

(27) Binetti, S.; Acciarri, M.; Brianza, A.; Saigni, C.; Pizzini, S. Effect of Oxygen Concentration on Diffusion Length in Czochralski and Magnetic Czochralski Silicon. *Materials Science and Technology* **1995**, *11*, 665-669.

(28) Joshi, S. M.; Gösele, U. M.; Tan, T. Y. Minority Carrier Diffusion Length Improvement Czochralski Silicon by Aluminum Gettering. *Mat. Res. Soc. Symp. Proc*. **1995**, *378*, 279-284.

(29) Plößl, A.; Kräuter, G. Wafer Direct Bonding: Tailoring Adhesion Between Brittle Materials. *Mat. Sci. Eng. R: Reports* **1999**, *25*, 1-2, 1-88.

(30) Born, M.; Wolf, E. Principles of Optics: Electromagnetic Theory of Propagation, Interference and Diffraction of Light. *Pergamon Press* **1964**.

(31) Baker-Finch, S.C.; McIntosh, K.R.; Yan, D.; Chern Fong, K.; Kho, T. C. Near-Infrared Free Carrier Absorption in Heavily Doped Silicon. *J. Appl. Phys* **2014**, *116*, 63106.

(32) Burger, T.; Sempere, C.; Roy-Layinde, B.; Lenert, A. Present Efficiencies and Future Opportunities in Thermophotovoltaics. *Joule* **2020**, *4*, 1660–1680.

(33) Saga, T. Advances in Crystalline Silicon Solar Cell Technology for Industrial Mass Production. *Npg. Asia Mate*r. **2010**, *2*, 96-102.

(34) Kern, W. The Evolution of Silicon Wafer Cleaning Technology. *J. Electrochem*. *Soc*. **1990**, *137*, 6, 1887.